© 2022. Published by The Company of Biologists Ltd | Journal of Cell Science (2023) 136, jcs259257. doi:10.1242/jcs.259257

SHORT REPORT

SPECIAL ISSUE: CELL BIOLOGY OF MOTORS

Transient accumulation and bidirectional movement of KIF13B in primary cilia

Alice Dupont Juhl[1,*], Zeinab Anvarian[2,*], Stefanie Kuhns[1], Julia Berges[2,3], Jens S. Andersen[1], Daniel Wüstner[1,‡] and Lotte B. Pedersen[2,‡]

ABSTRACT

Primary cilia are microtubule-based sensory organelles whose assembly and function rely on the conserved bidirectional intraflagellar transport (IFT) system, which is powered by anterograde kinesin-2 and retrograde cytoplasmic dynein-2 motors. Nematodes additionally employ a cell-type-specific kinesin-3 motor, KLP-6, which moves within cilia independently of IFT and regulates ciliary content and function. Here, we provide evidence that a KLP-6 homolog, KIF13B, undergoes bursts of bidirectional movement within primary cilia of cultured immortalized human retinal pigment epithelial (hTERT-RPE1) cells. Anterograde and retrograde intraciliary velocities of KIF13B were similar to those of IFT (as assayed using IFT172–eGFP), but intraciliary movement of KIF13B required its own motor domain and appeared to be cell-type specific. Our work provides the first demonstration of motor-driven, intraciliary movement by a vertebrate kinesin other than kinesin-2 motors.

KEY WORDS: KIF13B, Cilia, Extracellular vesicles, Intraflagellar transport, Kinesin-3

INTRODUCTION

Primary cilia are microtubule-based sensory organelles found on the surface of almost all animal cells and are pivotal for regulating diverse signaling pathways such as Sonic hedgehog (Shh) signaling and polycystin-1- and polycystin-2-mediated signaling (Anvarian et al., 2019). Cilia are compartmentalized organelles whose assembly, maintenance and function depend on the conserved intraflagellar transport (IFT) machinery that via kinesin-2 and cytoplasmic dynein-2 motors, brings IFT-A and IFT-B complexes with associated ciliary cargoes into and out of the organelle, respectively (Pedersen and Rosenbaum, 2008; Taschner and Lorentzen, 2016). Ciliary composition and function are additionally regulated by the ciliary transition zone (Garcia-Gonzalo and Reiter, 2016), vesicular trafficking and endocytosis of ciliary components (Pedersen et al., 2016; Blacque et al., 2017), and release of extracellular vesicles (EVs) from cilia or the periciliary membrane compartment (Wood and Rosenbaum, 2015; Akella and Barr, 2021).

Two types of ciliary kinesin-2 motors have been described: heterotrimeric kinesin-2 [comprising KIF3A, KIF3B and KAP3 (also known as KIFAP3) in vertebrates], which functions as the canonical anterograde IFT motor, and homodimeric kinesin-2 (KIF17 in vertebrates), which functions as an accessory anterograde IFT motor in some cilia (Pedersen and Rosenbaum, 2008; Prevo et al., 2017). Several additional kinesins have been shown to localize to and function at cilia, most of which regulate ciliary assembly and length by affecting microtubule dynamics (Reilly and Benmerah, 2019). A notable exception is the *Caenorhabditis elegans* kinesin-3 motor KLP-6, which moves independently of conventional IFT within male-specific sensory cilia and negatively affects the velocity of kinesin-2 motors (Morsci and Barr, 2011). KLP-6 also regulates ciliary targeting and EV-mediated release of polycystin-2 to control male mating behavior (Peden and Barr, 2005; Wang et al., 2014). Ciliary EVs act as signal-carrying entities in *C. elegans* and *Chlamydomonas* (Wang et al., 2014; Wood et al., 2013; Luxmi et al., 2019), and might rid the organelle of unwanted material in vertebrates (Nager et al., 2017; Phua et al., 2017). The precise mechanisms underlying release of EVs from cilia are unclear, but in addition to KLP-6, other factors implicated in this process include the BBSome complex, a retrograde IFT membrane cargo adaptor (Lechtreck, 2015; Nager et al., 2017; Akella et al., 2020), actin polymerization at the ciliary EV release site (Nager et al., 2017), and axonemal tubulin posttranslational modification (Akella and Barr, 2021). It is unknown whether vertebrate kinesin-3 motors move within primary cilia and promote ciliary EV release, and to date KLP-6 is the only kinesin, apart from IFT kinesin-2 motors, with demonstrated intraciliary motility.

We have previously shown that a KLP-6 homolog, KIF13B, localizes to primary cilia in mouse fibroblasts and immortalized human retinal pigment epithelial (hTERT-RPE1) cells, and that its depletion in these cells causes ciliary accumulation of the cholesterol-binding membrane protein CAV1 and impaired Shh signaling (Schou et al., 2017). The molecular basis for this phenotype was not clear, and it was unknown whether KIF13B actually moves within cilia. Here, we show, using live-cell imaging combined with image analysis and simulations, that KIF13B undergoes bursts of IFT-like bidirectional movement within primary cilia of hTERT-RPE1 cells. Anterograde and retrograde intraciliary velocities of KIF13B were similar to those of IFT (as assayed using IFT172–eGFP), but intraciliary movement of KIF13B required its own motor domain and appeared to be cell-type specific. Occasionally, EV-like release of KIF13B from the cilium tip was observed. Our results provide the first demonstration of intraciliary movement by a vertebrate kinesin other than IFT

[1]Department of Biochemistry and Molecular Biology, University of Southern Denmark, Campusvej 55, DK-5230 Odense M, Denmark. [2]Department of Biology, University of Copenhagen, Universitetsparken 13, DK-2100 Copenhagen Ø, Denmark. [3]Department of Biomedicine, Facultad Ciencias Experimentales, Universidad Francisco de Vitoria, Ctra. Pozuelo-Majadahonda Km. 1.800, 28223 Pozuelo de Alarcón, Madrid, Spain.
*These authors contributed equally to this work

‡Authors for correspondence (wuestner@bmb.sdu.dk; lbpedersen@bio.ku.dk)

J.S.A., 0000-0002-6091-140X; D.W., 0000-0003-4995-9709; L.B.P., 0000-0002-9749-3758

Handling Editor: David Glover
Received 11 August 2021; Accepted 1 April 2022

kinesin-2 motors, and of transient burst-like kinesin-driven motility within cilia of any organism.

RESULTS AND DISCUSSION

To investigate whether KIF13B moves inside cilia, we expressed a previously validated eGFP–KIF13B fusion protein (Schou et al., 2017; Serra-Marques et al., 2020) in hTERT-RPE1 cells stably expressing a red fluorescent ciliary membrane marker, SMO–tRFP (Lu et al., 2015), and starved cells of serum to induce ciliogenesis prior to analysis by confocal live-cell imaging. In all cells examined (n=54), eGFP–KIF13B was strongly concentrated at the ciliary base, and 15 of the cells additionally displayed rapid and transient accumulation of eGFP–KIF13B within the cilium itself (Fig. 1, Table 1; Movies 1, 2). Moreover, among the 15 cells showing intraciliary movement of eGFP–KIF13B, two cells additionally exhibited EV-like release of eGFP–KIF13B from the ciliary tip (Fig. 1A,D; Table 1; Movie 1). This rare phenomenon could be a side effect of the ciliary SMO–tRFP overexpression, as we did not observe it in hTERT-RPE1 cells expressing endogenously mScarlet-tagged ARL13B to mark cilia (Fig. S1D, Movie 3; Table 1), although we cannot exclude that EV-like tip release of eGFP–KIF13B might occur in the latter cells on rare occasions and/or under specific physiological conditions. Importantly, in 16% of the transfected ARL13B–mScarlet cells (n=38) eGFP–KIF13B did exhibit rapid and transient accumulation within cilia, as observed in the SMO–tRFP cells (Fig. S1D, Movie 3; Table 1), supporting that this behavior of eGFP–KIF13B was not a consequence of the ciliary membrane marker used. The proportion of transfected live hTERT-RPE1 cells displaying eGFP–KIF13B within cilia (16–37%; Table 1) is in line with our previous observations in fixed hTERT-RPE1 cells, where we detected eGFP–KIF13B in cilia of 23% of the transfected cells (Schou et al., 2017). Moreover, in the latter study, cells were pre-extracted with detergent containing AMP-PNP prior to fixation and immunofluorescence microscopy, supporting that eGFP–KIF13B is bound to axonemal microtubules within cilia (Schou et al., 2017).

Kymograph analysis indicated that eGFP–KIF13B moves bidirectionally within cilia at 0.64±0.07 µm/s in the anterograde direction (mean±s.e.m. of n=37 measurements from five cells) and 0.39±0.06 µm/s in the retrograde direction (mean±s.e.m. of n=36 measurements from five cells) (Fig. 1E,F; Fig. S1C). This is within the range of velocities reported for anterograde and retrograde IFT in mammalian cells (Williams et al., 2014) and for anterograde velocity of KLP-6 in *C. elegans* cephalic male (CEM) cilia (Morsci and Barr, 2011), but slower than the reported anterograde speed for KIF13B moving on cytoplasmic microtubules in HeLa cells (2–3 µm/s; Serra-Marques et al., 2020). Since kinesin velocity is influenced by multiple factors, including tubulin posttranslational modifications (Sirajuddin et al., 2014) and interaction with other motors (Snow et al., 2004; Morsci and Barr, 2011; Prevo et al., 2015; Milic et al., 2017), the unique structure and composition of the cilium may account for the slower KIF13B velocity in this compartment compared to that in the cell body. Nevertheless, kymographs indicated that eGFP–KIF13B moves progressively in both directions within cilia without slowing or acceleration and without prolonged pauses at the ciliary tip. From the cumulative histogram of velocities, we found that anterograde movement was slightly faster than retrograde movement (Fig. 1E,F). The cumulative histogram of velocities, v, was fitted to a Weibull distribution function of the form $y(v)=1-\exp[-(\alpha \cdot v)^{\beta}]$ with α=1.58 and β=2.11 for anterograde transport, and α=2.76 and β=2.94 for retrograde transport, suggesting a rather broad distribution of velocities (Fig. 1F). Image-based simulations of IFT indicated that movement of eGFP–KIF13B inside cilia with such velocities over the entire cilia length of more than 5 µm would result in oscillation frequencies for bidirectional movement of about 30 s (Fig. S2). The observed periodicity of intensity oscillations of eGFP–KIF13B in cilia was much slower – typically between 100 and 500 s (Fig. 1B,C; Movies 1, 2). This can be inferred from the example shown in Fig. 1A,B and is supported by an analysis of power spectra of this and similar intensity profiles (Fig. S1A,B). Such dynamic behavior likely reflects the import and export kinetics of KIF13B in primary cilia combined with frequent switching of directions. It is comparable to the avalanche-like injection of IFT particles into cilia, observed previously (Ludington et al., 2013), indicating that eGFP–KIF13B moves frequently up and down in cilia before eventually being exported from the cilium base into the cytosol or, in rare cases, released from the cilium tip.

In the amphid and phasmid sensory cilia of *C. elegans*, homodimeric (OSM-3) and heterotrimeric kinesin-2 motors function in coordination to mediate anterograde IFT in the axoneme middle segment, whereas OSM-3 alone mediates anterograde IFT in the distal segment (Snow et al., 2004). In male-specific *C. elegans* cilia, the kinesin-3 motor KLP-6 moves independently of OSM-3 and heterotrimeric kinesin-2 IFT motors, but KLP-6 appears to slow down both motors (Morsci and Barr, 2011). To investigate whether eGFP–KIF13B intraciliary motility is coordinated with conventional IFT, we first compared its dynamics to that of the IFT-B2 complex component IFT172 (Taschner et al., 2016), which we endogenously tagged with eGFP at its C terminus (IFT172–eGFP) in the hTERT-RPE1 cell line. We found that IFT172–eGFP moves bidirectionally along cilia in distinct spots, whose paths are clearly discernable in the video sequences and kymographs (Fig. 2A–D; Movie 4). Anterograde and retrograde movement of IFT172–eGFP was occasionally observed in parallel in the same cilium (Fig. 2C,D), and IFT172–eGFP was constantly present in cilia, in contrast to the periodic ciliary import and export observed for eGFP–KIF13B. Kymograph analysis indicated that IFT172–eGFP moves with an average velocity of 0.53±0.02 µm/s in the anterograde direction (mean±s.e.m. of n=75 measurements from five cells) and of 0.32±0.02 µm/s in the retrograde direction (mean ±s.e.m. of n=50 measurements from five cells). The cumulative histogram of velocities of IFT172–eGFP was also fitted to a Weibull distribution function, with α=1.58 and β=2.11 for anterograde transport, and α=2.83 and β=2.74 for retrograde transport (Fig. 2E). Both the mean values and the distribution function of measured velocities of IFT172–eGFP coincide very closely with the measured intraciliary velocities of eGFP–KIF13B in the hTERT-RPE1 SMO–tRFP cells. These results suggest that intraciliary movement of KIF13B is closely coordinated with conventional IFT. To further sustain this conclusion, we attempted to visualize intraciliary eGFP–KIF13B movement simultaneously with mCherry–IFT88, expressed stably in hTERT-RPE1 cells, but this was not feasible as cells expressing both fusion proteins failed to produce cilia. Therefore, we next carried out live-cell imaging analysis in hTERT-RPE1 cells expressing SMO–tRFP and treated with the dynein inhibitor ciliobrevin D (Firestone et al., 2012), which has previously been used to inhibit IFT in mammalian primary cilia (Ye et al., 2013). These analyses showed that eGFP–KIF13B localized within primary cilia of 27% of the transfected ciliobrevin D-treated cells (n=59), but no oscillatory movement of eGFP–KIF13B within cilia was detected under these conditions (Fig. 3A,B, Table 1; Movie 5). Instead, eGFP–KIF13B either very slowly entered cilia, as shown in Fig. 3A and Movie 5, or was exported over a time course of several minutes

Journal of Cell Science (2023) 136, jcs259257. doi:10.1242/jcs.259257

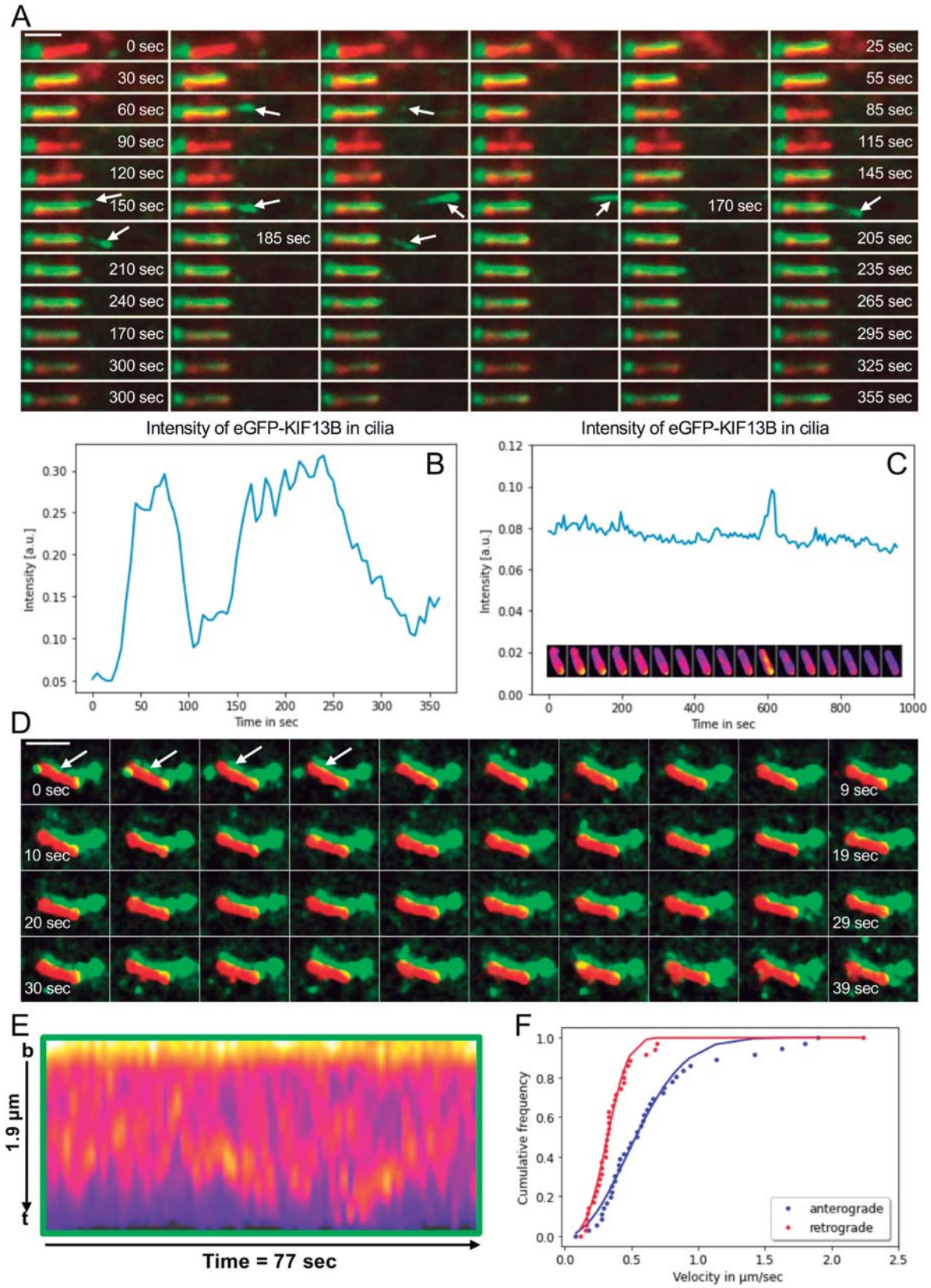

Fig. 1. See next page for legend.

Fig. 1. Transient bidirectional movement and EV-like tip release of eGFP–KIF13B in primary cilia of hTERT-RPE1 cells. (A) Time-lapse sequence showing eGFP–KIF13B (green) transiently moving into an hTERT-RPE1 cell cilium, which is marked with SMO–tRFP (red). In less than one minute, eGFP–KIF13B accumulates in the cilium, and some is released from the cilium tip (arrows) at 70–82 s and 155–185 s of the video sequence. Based on Movie 1. Images are representative of 15 cells. (B) Measurement of eGFP–KIF13B fluorescence intensity (a.u., arbitrary units) in a cilium over time, showing entry into the cilium in repeated bursts. (C) Example of an analysis similar to that shown in B, but with only one burst of eGFP–KIF13B observed. The inset images are example snapshots that are temporally aligned with the curve [color code is a FIRE look up table (LUT) in ImageJ with low intensities in blue, intermediate intensities in red and high intensities in yellow]. (D) Time-lapse sequence of another hTERT-RPE1 cell acquired with higher time resolution (interval time of 1.1 s), showing intraciliary movement of eGFP–KIF13B (green). The cilium is marked with SMO–tRFP (red). Arrows indicate movement of eGFP–KIF13B along the cilium. Based on Movie 2. Images are representative of 15 cells. Note that red and green images are slightly offset in A and D to better visualize movement of eGFP–KIF13B relative to SMO–tRFP. (E) Kymograph of a high-time-resolution sequence similar to that presented in D, showing eGFP–KIF13B intraciliary movement (see also Fig. S1C, which includes lines to mark anterograde and retrograde movements). The kymograph is color-coded to show fluorescence intensity of eGFP–KIF13B using a FIRE LUT, as described above (b, cilium base; t, cilium tip). (F) Cumulative frequency distributions of the velocity of anterograde and retrograde intraciliary movement of eGFP–KIF13B, based on, respectively, 37 and 36 measurements from 5 cells. Lines show fitted Weibull distribution functions of the form $y(v)=1-\exp[-(\alpha \cdot v)^{\beta}]$ with $\alpha=1.58$ and $\beta=2.11$ for anterograde transport and $\alpha=2.76$ and $\beta=2.94$ for retrograde transport, suggesting a rather broad distribution of eGFP–KIF13B velocities. Scale bars: 2 µm.

(data not shown). Since ciliobrevin D treatment leads to accumulation of stalled IFT trains on axonemal microtubules (Ye et al., 2013), we cannot conclude from these experiments whether eGFP–KIF13B is being moved by IFT, as the 'roadblock' effect of stalled IFT trains could impair eGFP–KIF13B intraciliary movement indirectly. To further investigate possible coordination of eGFP–KIF13B intraciliary movement with conventional IFT, quantitative live-cell imaging analysis was additionally performed using a truncated version of KIF13B lacking the motor domain (Lamason et al., 2010), hereafter referred to as motorless eGFP–KIF13B. This analysis demonstrated that motorless eGFP–KIF13B enters cilia in 26% of the transfected cells (n=27), but its fluorescence intensity was observed to be much lower in cilia than at the basal body, and bursts of intraciliary movement and ciliary tip release were not observed (Fig. 3C,D, Table 1; Movie 6). In contrast, similar analysis of a motorless version of homodimeric kinesin-2 KIF17 in cilia of mammalian olfactory sensory neurons has shown that motorless KIF17 can move along the entire axoneme by associating with heterotrimeric kinesin-2 motors (Williams et al., 2014). We conclude that intraciliary motility of KIF13B depends on its own motor domain and is closely coordinated with conventional IFT.

Next, we asked whether other kinesin-3 motors or known ciliary motors exhibit the same type of burst-like intraciliary motility as we observed for eGFP–KIF13B. The human genome encodes seven different kinesin-3 motors (Hirokawa et al., 2010), of which the KIF13 subgroup, comprising KIF13B and its proximal paralog KIF13A, displays the greatest sequence homology to the ciliary *C. elegans* KLP-6 kinesin-3 motor (Schou et al., 2017). When we analyzed eGFP–KIF13A movement in live hTERT-RPE1 cells expressing SMO–tRFP, we only detected eGFP–KIF13A in the cilium of a single transfected cell out of 18 cells analyzed (6%; Fig. S3A; Table 1), which is in agreement with our previously published results using fixed hTERT-RPE1 cells (Schou et al., 2017). In contrast, GFP-tagged KIF17, which functions as an accessory IFT kinesin-2 motor in some vertebrate cell types (Jenkins et al., 2006; Insinna et al., 2008; Williams et al., 2014), was stably localized at the ciliary tip in all cells examined (Fig. S3B; Table 1), as expected (Dishinger et al., 2010). Thus, amongst the motors tested, burst-like intraciliary motility was only observed for KIF13B.

To investigate whether intraciliary movement of KIF13B is cell-type specific, as is the case for *C. elegans* KLP-6 (Peden and Barr, 2005), we next performed live-cell imaging analysis of eGFP–KIF13B in ciliated mouse inner medullary collecting duct 3 (IMCD3) cells stably expressing mCherry–ARL13B. We found that eGFP–KIF13B localized to the base of, but not within, cilia of these cells (Fig. S3C; Table 1). It is unclear why eGFP–KIF13B failed to localize to cilia in mCherry–ARL13B-expressing IMCD3 cells; notably, in preliminary experiments we observed that mNeonGreen-tagged KIF13B localized to and moved within cilia of mouse cortical collecting duct (mCCD) cells (data not shown), suggesting that intraciliary movement of KIF13B is not limited to hTERT-RPE1 cells.

Table 1. Overview of live-cell imaging results in hTERT-RPE1 and IMCD3 cells, focusing on localization of GFP-tagged KIF proteins to the cilium–centrosome axis

			Number of cells with KIF fusion protein localizing to:		
Cell type and treatment	Fusion protein	*n*	Basal body	Cilium and basal body	Comment
hTERT-RPE1 SMO–tRFP	eGFP–KIF13B	54	39 (72%)	15 (28%)	Burst-like movement in cilia. EV-like release from cilia observed in two cases.
hTERT-RPE1 SMO–tRFP treated with ciliobrevin D	eGFP–KIF13B	59	38 (64%)	16 (27%)	Burst-like movement in one cilium.
hTERT-RPE1 SMO–tRFP treated with DMSO	eGFP–KIF13B	19	12 (63%)	7 (37%)	Burst-like movement in four cilia.
hTERT-RPE1 SMO–tRFP	motorless eGFP–KIF13B	26	19 (73%)	7 (27%)	No burst-like movement in cilia.
hTERT-RPE1 SMO–tRFP	eGFP–KIF13A	18	0	1 (6%)	–
hTERT-RPE1 SMO–tRFP	GFP–KIF17	2	0	2 (100%)	Stable localization at the cilium tip.
hTERT-RPE1 ARL13B–mScarlet	GFP–KIF17	14	0	14 (100%)	Stable localization at the cilium tip.
hTERT-RPE1 ARL13B–mScarlet	eGFP–KIF13B	38	32 (84%)	6 (16%)	Burst-like movement in cilia.
IMCD3 mCherry–ARL13B	eGFP–KIF13B	10	10 (100%)	0 (0%)	–
IMCD3 mCherry–ARL13B treated with purmorphamine	eGFP–KIF13B	16	16 (100%)	0 (0%)	–

n, number of live cells imaged per condition.

Journal of Cell Science (2023) 136, jcs259257. doi:10.1242/jcs.259257

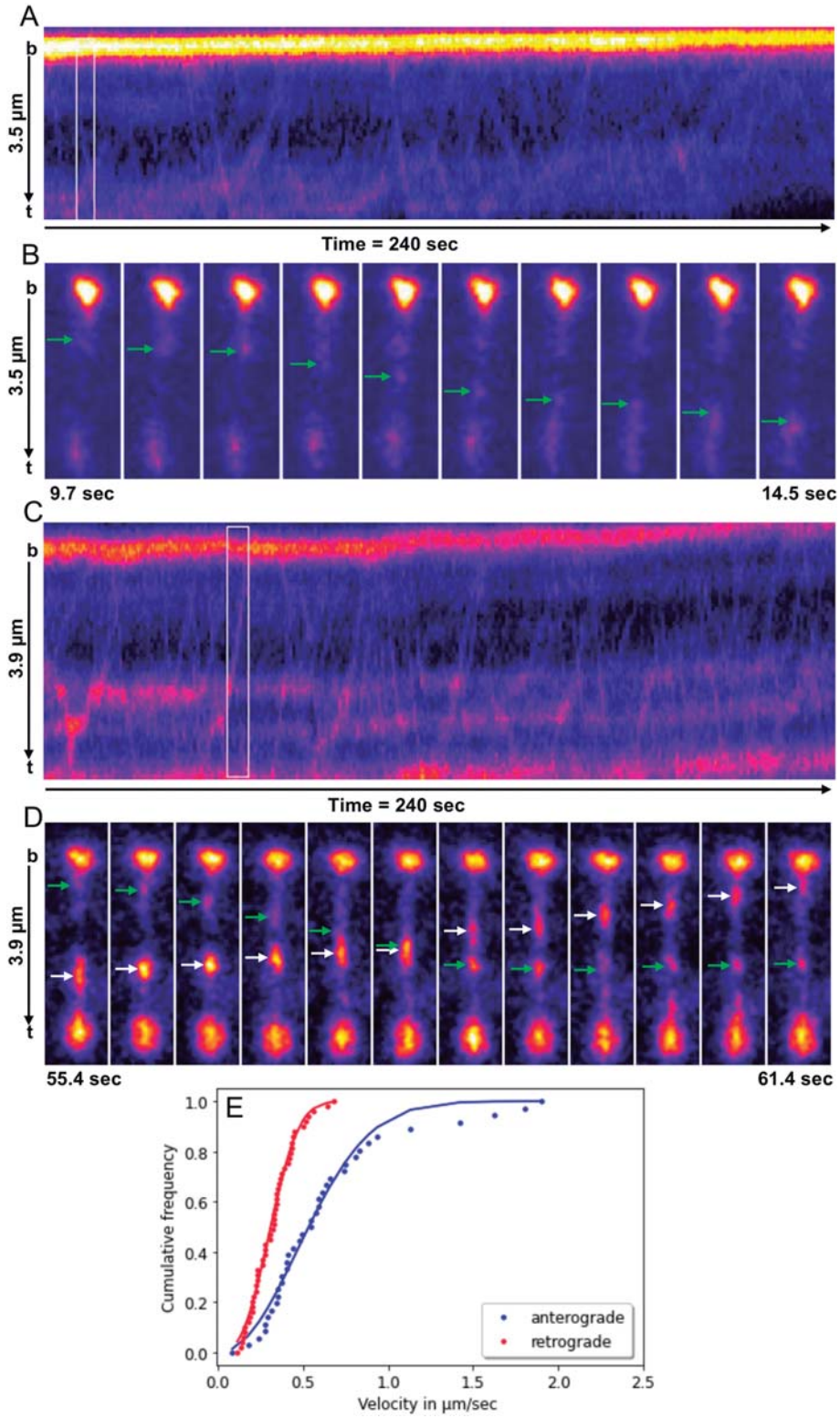

Fig. 2. Live-cell imaging analysis of IFT172–eGFP in cilia. (A,C) Kymographs depicting cilia of two hTERT-RPE1 cells stably expressing IFT172–eGFP and imaged with high temporal resolution (1.9 frames/s) using a confocal microscope with temperature control. Based on Movie 4. White boxes in A and C indicate regions shown in zoom images in B and D, respectively. Kymographs are color-coded using a FIRE LUT to show fluorescence intensities of IFT172–eGFP at the ciliary base and during its movement inside cilia (b, cilium base; t, cilium tip). The kymographs shown are representative of 5 cells. (B) Zoom of the kymograph shown in A, with anterograde movement of IFT172–eGFP from the cilia base to tip indicated by green arrows. (D) Zoom of the kymograph shown in panel C, with anterograde movement of IFT172–eGFP from the cilia base to tip (green arrows) crossing over with retrogradely moving IFT172–eGFP (white arrows). (E) Cumulative frequency distributions of the velocity of anterograde and retrograde intraciliary movement of IFT172–eGFP, based on, respectively, 75 and 50 measurements from 5 cells. Lines show fitted Weibull distribution functions of the form $y(v)=1-\exp[-(\alpha \cdot v)^{\beta}]$ with $\alpha=1.58$ and $\beta=2.11$ for anterograde transport and $\alpha=2.83$ and $\beta=2.74$ for retrograde transport.

In summary, our results demonstrate that eGFP–KIF13B transiently enters cilia and moves bidirectionally within the organelle at speeds reminiscent of IFT. Occasionally we observed EV-like release of eGFP–KIF13B from the ciliary tip. This phenomenon could be a side effect of the ciliary membrane marker used for imaging, but we cannot exclude that physiologically relevant release of KIF13B from cilia might occur under some circumstances, such as in response to physical (Wang et al., 2020) or chemical (Nager et al., 2017; Phua et al., 2017) stimuli. Intraciliary movement of eGFP–KIF13B requires its own motor domain and seems to be cell-type specific, as has been reported for KLP-6 in *C. elegans* (Morsci and Barr, 2011). Since KIF13B is a plus end-directed motor and moves bidirectionally within cilia at

Journal of Cell Science (2023) 136, jcs259257. doi:10.1242/jcs.259257

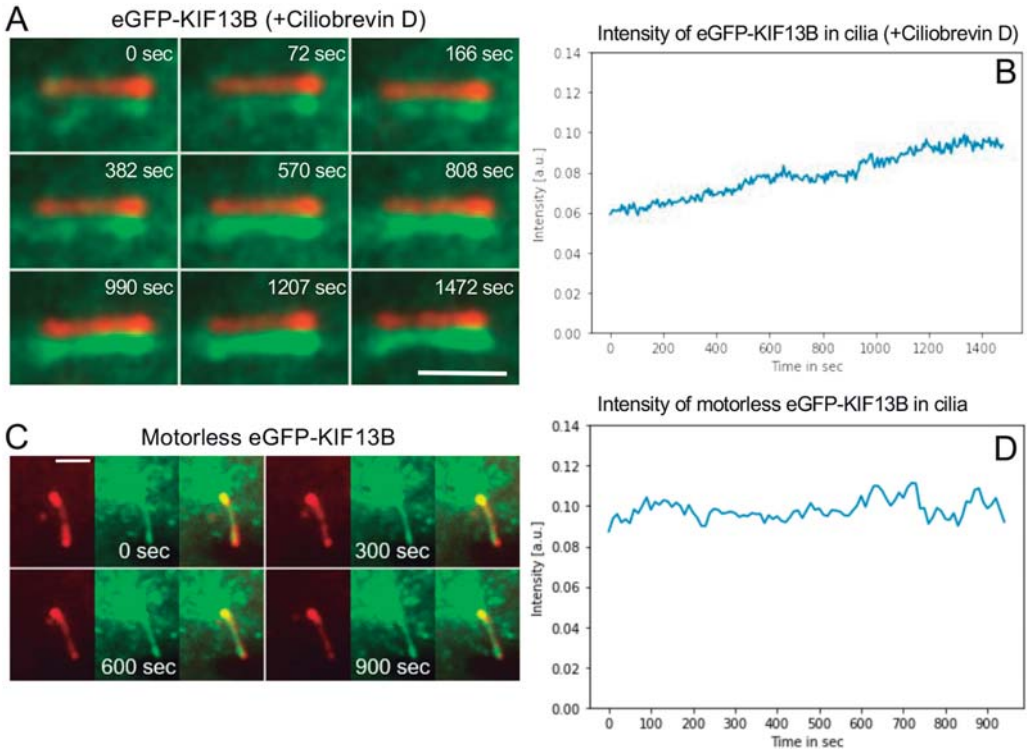

Fig. 3. Ciliary movement of eGFP–KIF13B requires its own motor domain. (A) Snapshots taken from Movie 5 showing cilium localization of eGFP–KIF13B (green) in hTERT-RPE1 cells expressing SMO–tRFP (red) and treated with 10 µM ciliobrevin D for 1–6 h. Note that red and green images are slightly offset in A to better visualize movement of eGFP–KIF13B relative to SMO–tRFP. Images are representative of 16 cells. Scale bar: 2 µm. (B) Measurement of eGFP–KIF13B fluorescence intensity (a.u., arbitrary units) in cilia of the ciliobrevin D-treated cell shown in A as a function of time (see Movie 5). (C) Snapshots taken from Movie 6 showing motorless eGFP–KIF13B (green) in hTERT-RPE1 cells expressing SMO–tRFP (red). eGFP–KIF13B accumulates around the ciliary base, with some localizing stably to cilia over time (*n*=25 cells). Scale bar: 2 µm. (D) Measurement of motorless eGFP–KIF13B fluorescence intensity in cilia of the cell shown in C over time (see Movie 6).

similar velocities to IFT172, its retrograde movement must be mediated via association with the dynein-2-driven retrograde IFT machinery. Anterograde movement of KIF13B within cilia is likely powered by its own intrinsic motor activity, yet it is coordinated with kinesin-2 motors and conventional IFT. We also cannot exclude that the KIF13B motor domain is required for interaction with the IFT machinery. In future studies it will be interesting to further dissect the coordination of KIF13B intraciliary movement with IFT – for example, by using single molecule imaging technologies – and to determine the ciliary cargoes of KIF13B.

MATERIALS AND METHODS

Plasmids, mammalian cell culture, stable cell lines and transfection

The following previously described plasmids were used: eGFP–KIF13B (Asaba et al., 2003), motorless eGFP–KIF13B (Lamason et al., 2010), eGFP–KIF13A (Schou et al., 2017), GFP–KIF17 (Jaulin and Kreitzer, 2010), pcDNA3.1(+) (Thermo Fisher Scientific), pCAG-enAsCas12a (Addgene plasmid 107941) (Kleinstiver et al., 2019), pMaCTag-Z12 (Addgene plasmid 120055) and pMaCTag-P05 (Addgene plasmid 120016) (Fueller et al., 2020). Plasmids were propagated in *Escherichia coli* DH10B cells using standard procedures and purified using NucleoBond Xtra Midi EF Kit (Macherey-Nagel).

hTERT-RPE1 cells stably expressing SMO–tRFP were generously provided by Christopher J. Westlake (Center for Cancer Research, National Cancer Institute, National Institutes of Health, Frederick, MD 21702, USA) and have been described previously (Lu et al., 2015). To establish the hTERT-RPE1 cell lines with ARL13B–mScarlet or IFT172–eGFP tagged at the endogenous locus, we used a CRISPR/Cas12a-assisted PCR tagging approach (Fueller et al., 2020). Briefly, repair donor templates were generated by PCR with gene-specific primers and the plasmids pMaCTag-Z12 or pMaCTag-P05. The PCR template cassette together with the enAsCas12a expression plasmid were electroporated into hTERT-RPE1 cells using the Neon Transfection System (Thermo Fisher Scientific), and cells were selected with zeocin or puromycin for 2 weeks. Isolated single-cell clones were characterized by live-cell imaging, PCR and Sanger sequencing. The hTERT-RPE1 SMO–tRFP cells were cultured in Dulbecco's Modified Eagle Medium (DMEM; Thermo Fisher Scientific) supplemented with 10% fetal bovine serum (FBS; Thermo Fisher Scientific), 1% penicillin-streptomycin (Thermo Fisher Scientific), and 10 µg/ml hygromycin B. hTERT-RPE1 ARL13B–mScarlet and hTERT-RPE1 IFT72–eGFP cells were cultured in DMEM/F12 medium (Thermo Fisher Scientific) supplemented with 10% FBS (Gibco), 1% Glutamax (Gibco) and 1% penicillin-streptomycin. hTERT-RPE1 cells stably expressing mCherry–IFT88 were generated from lentiviral transduction using plasmids described previously (Campeau et al., 2009). The IFT88 open-reading frame was first amplified using PCR (forward primer, 5′-CCGGTACCATGATGCAAAATGTGCACCTGGC-3′; reverse primer, 5′-CCGCGGCCGCTTATTCTGGAAGCAAATCATCTCCTAAT-3′) from pCAG2-mChe-IFT88 (Kobayashi et al., 2021), generously provided by Kazuhisa Nakayama (Department of Physiological Chemistry, Graduate School of Pharmaceutical Sciences, Kyoto University, Sakyo-ku, Kyoto, Japan). PCR products were cloned into the Gateway system-compatible pENTR-mCherry-C1. Subsequently, pENTR-mCherry-IFT88 was recombined with pCDH-EF1a-Gateway-IRES-BLAST plasmid with LR recombination (Invitrogen/Thermo Fisher Scientific). Pools of hTERT-RPE1 cells stably expressing mCherry-IFT88 were selected with blasticidin (Sigma). For ciliobrevin D experiments, culture medium was exchanged with M1 medium (150 mM $NaCl_2$, 5 mM KCl, 1 mM $CaCl_2$, 1 mM $MgCl_2$, 5 mM glucose and 20 mM HEPES) containing 10 µM ciliobrevin D (Merck) in DMSO. Imaging was started after 1 h, and control cells treated with a similar volume of DMSO were analyzed in parallel.

Mouse IMCD3 cells stably expressing mCherry–ARL13B were a generous gift from Peter Gorilak and Vladimir Varga (Laboratory of Cell Motility, Institute of Molecular Genetics of the Czech Academy of Sciences, Prague, Czech Republic). These cells were cultured in DMEM/F12 medium (Thermo Fisher Scientific) containing 10% heat-inactivated FBS and 1% penicillin-streptomycin.

For the imaging experiments, cells were seeded on glass-bottom dishes (35/22 mm; HBSt-3522; WillCo Wells) or on 35 mm microscope dishes with glass bottom (MatTek; P35G-1.5–50-C). Cells were transfected with KIF-encoding plasmid and empty vector pcDNA3.1(+) (1 µg total DNA) using 2 µl Lipofectamine 3000 reagent and 2 µl P3000 (Thermo Fisher Scientific). hTERT-RPE1 cells stably expressing SMO–tRFP were transfected a day after seeding, and IMCD3 cells expressing mCherry–ARL13B were reverse transfected at the time of seeding. To induce ciliogenesis, cells were cultured overnight (16 h) in a medium free of FBS and antibiotics. Serum starvation started at 2 h post transfection for hTERT-RPE1 cells and at 16 h post transfection for IMCD3 cells. To activate the Shh pathway and promote SMO ciliary entrance in IMCD3 cells, the cells were serum starved with DMEM/F12 medium containing 2 µM purmorphamine (Sigma, SML0868). Cell lines were routinely authenticated and checked for contamination.

Live-cell fluorescence imaging

Live-cell imaging was carried out on several confocal microscopes, all of which allowed temperature (37°C) and CO_2 (5%) regulation in a humidity chamber. These included a fully motorized Olympus IX83 inverted microscope equipped with a spinning disk (Yokogawa) and a Hamamatsu ORCA-Flash 4.0 digital camera (C13440); and a motorized inverted Nikon–Andor spinning-disk microscope equipped with CSU-X1 spinning disk (Yokogawa) and/or laser launcher, Okolab microscope stage incubator, and a perfect focus system (PFS) (at DaMBIC, University of Southern Denmark). Both 60× and 100× numerical aperture (NA) 1.4 oil objectives (Olympus) were used. The 488 nm and 561 nm laser lines were used for imaging eGFP and tRFP, respectively. The time-lapse sequences were obtained with time intervals ranging from 5 to 10 s. For laser scanning confocal microscopy at DaMBIC, University of Southern Denmark, a Nikon Ti-2, A1 LFO confocal microscope with a Plan Apo λ 100× NA 1.4 oil objective with the following excitation/emission settings was used: 488/525 nm for eGFP and 561/595 nm for tRFP and mScarlet. The interval for the time-lapse sequences ranged from 0.5 to 10 s. All live-cell imaging was carried out in DMEM or M1 medium. During imaging experiments, we carefully selected those cells that had a low expression level of eGFP–KIF13B (or other kinesin fusion proteins) but could still be visualized using our microscopes. In most cases, cells overexpressing eGFP–KIF13B lose their primary cilia because of the negative effect of this protein on the cilia length, as reported previously (Schou et al., 2017).

Image analysis and simulations

All image analysis and simulations were carried out in ImageJ (https://imagej.nih.gov/ij/), either using existing plugins or implemented as self-developed macro scripts (available from the authors upon request). Subsequent time-series analysis was implemented as Jupyter notebooks in Python (https://jupyter.org/). First, the cilia intensity of eGFP-tagged KIF13B (wild type or motorless mutant) was isolated based on the red fluorescent marker protein SMO–tRFP. For that, a rectangular region of interest (ROI) was defined around the red cilia marker, and an intensity threshold was applied to the SMO–tRFP fluorescence in cilia weighted by the mean intensity of the red marker in the entire ROI. This procedure accounted for eventual photobleaching and secured a stable cilia area segmentation. A binary mask comprising the cilia area with intensities of either 0 or 1 was generated and multiplied with the corresponding green image series of the eGFP-tagged KIF13B. Integrated fluorescence intensity of eGFP–KIF13B was measured from videos with long acquisition time (5–6 s, acquired using a spinning-disk confocal system) and normalized to the total green fluorescence in the rectangular ROI. To determine periodicities in cilia location dynamics of eGFP–KIF13B, the extracted intensity time series was transformed into frequency space using the Fast Fourier transform function of the SciPy library in Python. Time-lapse sequences with shorter acquisition time (1.1 s intervals) were treated identically, but in addition to calculating integrated intensities, a kymograph analysis was carried out. For that, the segmented cilia were first spatially aligned using a rigid-body registration procedure. A 3-pixel-wide line (straight or segmented) was used, and the was kymograph calculated using the Multikymograph plugin of ImageJ developed by Drs A. Seitz [European Molecular Biology Laboratory (EMBL), Heidelberg, Germany] and J. Rietdorf (Friedrich Miescher Institute for Biomedical Research, Basel, Switzerland). Straight lines were identified, and velocities of eGFP–KIF13B were calculated using the accompanying macro script based on the known pixel size and interval time. Cumulative histograms of velocities measured in the anterograde and retrograde direction were calculated and fitted to a Weibull function as described in the Results and Discussion section. Image simulations of cilia movement were implemented as an ImageJ macro, using a fixed cilia length of 5 µm, a simulated pixel size of either 0.05 or 0.1 µm and a frame rate of 1 frame per second (1 Hz). A variable number of consecutive motors was translated towards the cilia tip with a constant speed. A stochastic velocity component was added from a uniform distribution, comprising ∼0–10% of the total velocity, to account for the stochastic nature of motor movement. Simulated images were convoluted with a Gaussian filter of width equal to 0.15 or 0.25 µm and Gaussian noise was added to account for blurring by the microscope optics and the camera read-out noise, respectively.

Acknowledgements

We thank Drs Christopher J. Westlake, Valdimir Varga, Athar Chisthi, Joel Pomerantz, Geri Kreitzer, Kazuhisa Nakayama, Michael Knop, Keith Joung and Benjamin Kleinstiver for reagents, and Søren Johansen for technical assistance. We thank the Danish Molecular Biomedical Imaging Center, University of Southern Denmark, for use of imaging equipment, supported by Novo Nordisk Foundation (NNF18SA0032928).

Competing interests

The authors declare no competing or financial interests.

Author contributions

Conceptualization: D.W., L.B.P.; Methodology: S.K., D.W.; Validation: A.D.J., Z.A., J.B.; Formal analysis: A.D.J., Z.A., D.W.; Investigation: A.D.J., Z.A., J.B., D.W.; Writing - original draft: L.B.P.; Writing - review & editing: A.D.J., Z.A., S.K., J.S.A., D.W.; Visualization: A.D.J., Z.A., D.W.; Supervision: Z.A., J.S.A., D.W., L.B.P.; Project administration: L.B.P.; Funding acquisition: J.S.A., D.W., L.B.P.

Funding

This work was supported by grants from Novo Nordisk Fonden (NNF18OC0053024, NNF15OC0016886 and NNF14OC0011535), Kræftens Bekæmpelse (R146-A9590) and Hartmann Fonden (A31662) to L.B.P. J.B. was supported by an Eramus+ traineeship from the European Commission. D.W. acknowledges funding from the Villum Fonden (grant 35865). J.S.A. and S.K. acknowledge support from Danmarks Frie Forskningsfond (grant 8021-00425B).

Peer review history

The peer review history is available online at https://journals.biologists.com/jcs/article-lookup/doi/10.1242/jcs.259257.

References

Akella, J. S. and Barr, M. M. (2021). The tubulin code specializes neuronal cilia for extracellular vesicle release. *Dev. Neurobiol.* **81**, 231-252. doi:10.1002/dneu.22787

Akella, J. S., Carter, S. P., Nguyen, K., Tsiropoulou, S., Moran, A. L., Silva, M., Rizvi, F., Kennedy, B. N., Hall, D. H., Barr, M. M. et al. (2020). Ciliary Rab28 and the BBSome negatively regulate extracellular vesicle shedding. *eLife* **9**, e50580. doi:10.7554/eLife.50580

Anvarian, Z., Mykytyn, K., Mukhopadhyay, S., Pedersen, L. B. and Christensen, S. T. (2019). Cellular signalling by primary cilia in development, organ function and disease. *Nat. Rev. Nephrol.* **15**, 199-219. doi:10.1038/s41581-019-0116-9

Asaba, N., Hanada, T., Takeuchi, A. and Chishti, A. H. (2003). Direct interaction with a kinesin-related motor mediates transport of mammalian discs large tumor suppressor homologue in epithelial cells. *J. Biol. Chem.* **278**, 8395-8400. doi:10.1074/jbc.M210362200

Blacque, O. E., Scheidel, N. and Kuhns, S. (2017). Rab GTPases in cilium formation and function. *Small GTPases*, **9**, 76-94. doi:10.1080/21541248.2017.1353847

Campeau, E., Ruhl, V. E., Rodier, F., Smith, C. L., Rahmberg, B. L., Fuss, J. O., Campisi, J., Yaswen, P., Cooper, P. K. and Kaufman, P. D. (2009). A versatile viral system for expression and depletion of proteins in mammalian cells. *PLoS ONE* **4**, e6529. doi:10.1371/journal.pone.0006529

Dishinger, J. F., Kee, H. L., Jenkins, P. M., Fan, S., Hurd, T. W., Hammond, J. W., Truong, Y. N., Margolis, B., Martens, J. R. and Verhey, K. J. (2010). Ciliary entry of the kinesin-2 motor KIF17 is regulated by importin-β2 and RanGTP. *Nat. Cell Biol.* **12**, 703-710. doi:10.1038/ncb2073

Firestone, A. J., Weinger, J. S., Maldonado, M., Barlan, K., Langston, L. D., O'Donnell, M., Gelfand, V. I., Kapoor, T. M. and Chen, J. K. (2012). Small-molecule inhibitors of the AAA+ ATPase motor cytoplasmic dynein. *Nature* **484**, 125-129. doi:10.1038/nature10936

Fueller, J., Herbst, K., Meurer, M., Gubicza, K., Kurtulmus, B., Knopf, J. D., Kirrmaier, D., Buchmuller, B. C., Pereira, G., Lemberg, M. K. et al. (2020). CRISPR-Cas12a-assisted PCR tagging of mammalian genes. *J. Cell Biol.* **219**, e201910210. doi:10.1083/jcb.201910210

Garcia-Gonzalo, F. R. and Reiter, J. F. (2016). Open sesame: how transition fibers and the transition zone control ciliary composition. *Cold Spring Harb. Perspect. Biol.* **9**, a028134. doi:10.1101/cshperspect.a028134

Hirokawa, N., Niwa, S. and Tanaka, Y. (2010). Molecular motors in neurons: transport mechanisms and roles in brain function, development, and disease. *Neuron* **68**, 610-638. doi:10.1016/j.neuron.2010.09.039

Insinna, C., Pathak, N., Perkins, B., Drummond, I. and Besharse, J. C. (2008). The homodimeric kinesin, Kif17, is essential for vertebrate photoreceptor sensory outer segment development. *Dev. Biol.* **316**, 160-170. doi:10.1016/j.ydbio.2008.01.025

Jaulin, F. and Kreitzer, G. (2010). KIF17 stabilizes microtubules and contributes to epithelial morphogenesis by acting at MT plus ends with EB1 and APC. *J. Cell. Biol.* **190**, 443-460. doi:10.1083/jcb.201006044

Jenkins, P. M., Hurd, T. W., Zhang, L., Mcewen, D. P., Brown, R. L., Margolis, B., Verhey, K. J. and Martens, J. R. (2006). Ciliary targeting of olfactory CNG channels requires the CNGB1b subunit and the kinesin-2 motor protein, KIF17. *Curr. Biol.* **16**, 1211-1216. doi:10.1016/j.cub.2006.04.034

Kleinstiver, B. P., Sousa, A. A., Walton, R. T., Tak, Y. E., Hsu, J. Y., Clement, K., Welch, M. M., Horng, J. E., Malagon-Lopez, J., Scarfò, I. et al. (2019). Engineered CRISPR-Cas12a variants with increased activities and improved targeting ranges for gene, epigenetic and base editing. *Nat. Biotechnol.* **37**, 276-282. doi:10.1038/s41587-018-0011-0

Kobayashi, T., Ishida, Y., Hirano, T., Katoh, Y. and Nakayama, K. (2021). Cooperation of the IFT-A complex with the IFT-B complex is required for ciliary retrograde protein trafficking and GPCR import. *Mol. Biol. Cell* **32**, 45-56. doi:10.1091/mbc.E20-08-0556

Lamason, R. L., Kupfer, A. and Pomerantz, J. L. (2010). The dynamic distribution of CARD11 at the immunological synapse is regulated by the inhibitory Kinesin GAKIN. *Mol. Cell* **40**, 798-809. doi:10.1016/j.molcel.2010.11.007

Lechtreck, K. F. (2015). IFT-cargo interactions and protein transport in Cilia. *Trends Biochem. Sci.* **40**, 765-778. doi:10.1016/j.tibs.2015.09.003

Lu, Q., Insinna, C., Ott, C., Stauffer, J., Pintado, P. A., Rahajeng, J., Baxa, U., Walia, V., Cuenca, A., Hwang, Y. S. et al. (2015). Early steps in primary cilium assembly require EHD1/EHD3-dependent ciliary vesicle formation. *Nat. Cell Biol.* **17**, 531. doi:10.1038/ncb3155

Ludington, W. B., Wemmer, K. A., Lechtreck, K. F., Witman, G. B. and Marshall, W. F. (2013). Avalanche-like behavior in ciliary import. *Proc. Natl. Acad. Sci. USA* **110**, 3925-3930. doi:10.1073/pnas.1217354110

Luxmi, R., Kumar, D., Mains, R. E., King, S. M. and Eipper, B. A. (2019). Cilia-based peptidergic signaling. *PLoS Biol.* **17**, e3000566. doi:10.1371/journal.pbio.3000566

Milic, B., Andreasson, J. O. L., Hogan, D. W. and Block, S. M. (2017). Intraflagellar transport velocity is governed by the number of active KIF17 and KIF3AB motors and their motility properties under load. *Proc. Natl. Acad. Sci. USA* **114**, E6830-E6838. doi:10.1073/pnas.1708157114

Morsci, N. S. and Barr, M. M. (2011). Kinesin-3 KLP-6 regulates intraflagellar transport in male-specific cilia of Caenorhabditis elegans. *Curr. Biol.* **21**, 1239-1244. doi:10.1016/j.cub.2011.06.027

Nager, A. R., Goldstein, J. S., Herranz-Pérez, V., Portran, D., Ye, F., Garcia-Verdugo, J. M. and Nachury, M. V. (2017). An actin network dispatches ciliary GPCRs into extracellular vesicles to modulate signaling. *Cell* **168**, 252-263.e14. doi:10.1016/j.cell.2016.11.036

Peden, E. M. and Barr, M. M. (2005). The KLP-6 kinesin is required for male mating behaviors and polycystin localization in *Caenorhabditis elegans*. *Curr. Biol.* **15**, 394-404. doi:10.1016/j.cub.2004.12.073

Pedersen, L. B. and Rosenbaum, J. L. (2008). Intraflagellar transport (IFT) role in ciliary assembly, resorption and signalling. *Curr. Top. Dev. Biol.* **85**, 23-61. doi:10.1016/S0070-2153(08)00802-8

Pedersen, L. B., Mogensen, J. B. and Christensen, S. T. (2016). Endocytic control of cellular signaling at the primary cilium. *Trends Biochem. Sci.* **41**, 784-797. doi:10.1016/j.tibs.2016.06.002

Phua, S. C., Chiba, S., Suzuki, M., Su, E., Roberson, E. C., Pusapati, G. V., Setou, M., Rohatgi, R., Reiter, J. F., Ikegami, K. et al. (2017). Dynamic remodeling of membrane composition drives cell cycle through primary cilia excision. *Cell* **168**, 264-279.e15. doi:10.1016/j.cell.2016.12.032

Prevo, B., Mangeol, P., Oswald, F., Scholey, J. M. and Peterman, E. J. (2015). Functional differentiation of cooperating kinesin-2 motors orchestrates cargo import and transport in C. elegans cilia. *Nat. Cell Biol.* **17**, 1536-1545. doi:10.1038/ncb3263

Prevo, B., Scholey, J. M. and Peterman, E. J. G. (2017). Intraflagellar transport: mechanisms of motor action, cooperation, and cargo delivery. *FEBS J.* **284**, 2905-2931. doi:10.1111/febs.14068

Reilly, M. L. and Benmerah, A. (2019). Ciliary kinesins beyond IFT: cilium length, disassembly, cargo transport and signalling. *Biol. Cell* **111**, 79-94. doi:10.1111/boc.201800074

Schou, K. B., Mogensen, J. B., Nielsen, B. S., Morthorst, S. K., Aleliunaite, A., Serra-Marques, A. M. A., Saunier, S., Bizet, A., Veland, I. R., Akhmanova, A. et al. (2017). KIF13B establishes a CAV1-enriched microdomain at the ciliary transition zone to promote Sonic hedgehog signaling. *Nat. Commun.* **8**, 14177. doi:10.1038/ncomms14177

Serra-Marques, A., Martin, M., Katrukha, E. A., Grigoriev, I., Peeters, C. A., Liu, Q., Hooikaas, P. J., Yao, Y., Solianova, V., Smal, I. et al. (2020). Concerted action of kinesins KIF5B and KIF13B promotes efficient secretory vesicle transport to microtubule plus ends. *eLife* **9**, e61302. doi:10.7554/eLife.61302

Sirajuddin, M., Rice, L. M. and Vale, R. D. (2014). Regulation of microtubule motors by tubulin isotypes and post-translational modifications. *Nat. Cell Biol.* **16**, 335-344. doi:10.1038/ncb2920

Snow, J. J., Ou, G., Gunnarson, A. L., Walker, M. R. S., Zhou, H. M., Brust-Mascher, I. and Scholey, J. M. (2004). Two anterograde intraflagellar transport motors cooperate to build sensory cilia on *C. elegans* neurons. *Nat. Cell Biol.* **6**, 1109-1113. doi:10.1038/ncb1186

Taschner, M. and Lorentzen, E. (2016). The intraflagellar transport machinery. *Cold Spring Harb. Perspect. Biol.* **8**, a028092. doi:10.1101/cshperspect.a028092

Taschner, M., Weber, K., Mourão, A., Vetter, M., Awasthi, M., Stiegler, M., Bhogaraju, S. and Lorentzen, E. (2016). Intraflagellar transport proteins 172, 80, 57, 54, 38, and 20 form a stable tubulin-binding IFT-B2 complex. *EMBO J.* **35**, 773-790. doi:10.15252/embj.201593164

Wang, J., Silva, M., Haas, L. A., Morsci, N. S., Nguyen, K. C., Hall, D. H. and Barr, M. M. (2014). C. elegans ciliated sensory neurons release extracellular vesicles that function in animal communication. *Curr. Biol.* **24**, 519-525. doi:10.1016/j.cub.2014.01.002

Wang, J., Nikonorova, I. A., Gu, A., Sternberg, P. W. and Barr, M. M. (2020). Release and targeting of polycystin-2-carrying ciliary extracellular vesicles. *Curr. Biol.* **30**, R755-R756. doi:10.1016/j.cub.2020.05.079

Williams, C. L., Mcintyre, J. C., Norris, S. R., Jenkins, P. M., Zhang, L., Pei, Q., Verhey, K. and Martens, J. R. (2014). Direct evidence for BBSome-associated intraflagellar transport reveals distinct properties of native mammalian cilia. *Nat. Commun.* **5**, 5813. doi:10.1038/ncomms6813

Wood, C. R. and Rosenbaum, J. L. (2015). Ciliary ectosomes: transmissions from the cell's antenna. *Trends Cell Biol.* **25**, 276-285. doi:10.1016/j.tcb.2014.12.008

Wood, C. R., Huang, K., Diener, D. R. and Rosenbaum, J. L. (2013). The cilium secretes bioactive ectosomes. *Curr Biol.* **23**, 906-911. doi:10.1016/j.cub.2013.04.019

Ye, F., Breslow, D. K., Koslover, E. F., Spakowitz, A. J., Nelson, W. J. and Nachury, M. V. (2013). Single molecule imaging reveals a major role for diffusion in the exploration of ciliary space by signaling receptors. *eLife* **2**, e00654.doi:10.7554/eLife.00654.025